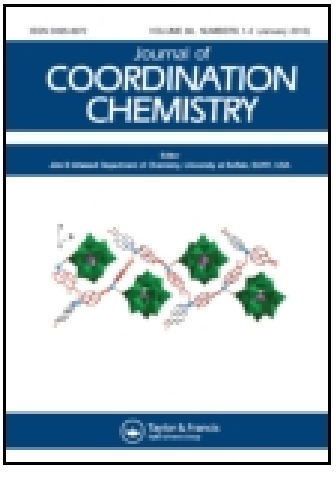

Journal of Coordination Chemistry
Publication details, including instructions for authors and subscription information:
http://www.tandfonline.com/loi/gcoo20

Six cation-templated halometal complexes and C-H activation of alkylene-bridged azoles

Haijuan Du[a], Wenzhen Fu[a], Siwen Zhang[b], Li Li[a], Hongmei Wang[a], Zhongcheng Yue[a], Wenli Zhang[a], Yunyin Niu[a] & Yu Zhu[a]

[a] College of Chemical and Molecular Engineering, Zhengzhou University, Zhengzhou, PR China

[b] College of Chemistry, Northeast Normal University, Changchun, China

Accepted author version posted online: 25 Mar 2014.Published online: 22 Apr 2014.

To cite this article: Haijuan Du, Wenzhen Fu, Siwen Zhang, Li Li, Hongmei Wang, Zhongcheng Yue, Wenli Zhang, Yunyin Niu & Yu Zhu (2014) Six cation-templated halometal complexes and C-H activation of alkylene-bridged azoles, Journal of Coordination Chemistry, 67:5, 807-821, DOI: 10.1080/00958972.2014.908288

To link to this article: http://dx.doi.org/10.1080/00958972.2014.908288

Journal of Coordination Chemistry, 2014
Vol. 67, No. 5, 807–821, http://dx.doi.org/10.1080/00958972.2014.908288

Six cation-templated halometal complexes and C–H activation of alkylene-bridged azoles

HAIJUAN DU†, WENZHEN FU†, SIWEN ZHANG‡, LI LI†, HONGMEI WANG†, ZHONGCHENG YUE†, WENLI ZHANG†, YUNYIN NIU*† and YU ZHU†

†College of Chemical and Molecular Engineering, Zhengzhou University, Zhengzhou, PR China
‡College of Chemistry, Northeast Normal University, Changchun, China

(*Received 13 October 2012; accepted 1 February 2014*)

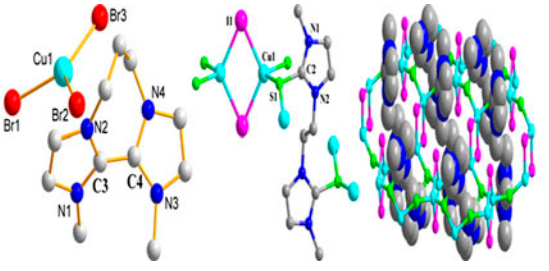

Four bis(*N*-heterocyclic carbene) precursors together with the cyclization and thiolation products were utilized to construct six dication-templated metal halides from 0,1 to 2-D polypseudorotaxane.

Six dication-templated complexes were discovered in efforts to investigate the effect of linear imidazolium-based template, 1,ω-bis(3,3′-methylimidazolium)alkyl dibromide, on pure inorganic halometal clusters. Complexes $\{[C_4(Mim)_2](Pb_2I_6)\}_n$ (**1**) ($\omega = 4$), $\{[C_1(Mim)_2](Ag_2I_4)\}_n$ (**2**) ($\omega = 1$), $\{[C_3(Mim)_2](Ag_2I_4)\}_n$ (**3**) ($\omega = 3$), and $\{[C_4(Mim)_2](Ag_2I_4)\}_n$ (**4**) ($\omega = 4$) possess 1-D chain architecture with different organic cations trapped in it. Compound $\{[C_3'(Mim)_2](CuBr_3)\}$ (**5**) ($\omega = 3$) contains the mononuclear anion $(CuBr_3)^{2-}$ and intra-molecular coupled organic cation with the formed seven-membered ring. $\{[C_2(Mim)_2S_2]_2(Cu_2I_2)\}_n$ (**6**) ($\omega = 2$) presents an infinite 2-D coordination polymer as the first representative polyrotaxane example featuring the biimidazolium thiolate cation ligand. All compounds were further characterized with IR spectra and thermal analysis properties.

Keywords: Template effect; N-substituted imidazolium salt; Halometal cluster; Crystal structures

1. Introduction

Template-oriented organic–inorganic hybrid materials have attracted interest owing to variety in topologies, fascinating properties and potential applications in catalysis, medicine, materials, and magnetochemistry [1–3]. Among the various families of inorganic–organic

*Corresponding author. Email: niuyy@zzu.edu.cn

hybrid polymers, haloclusters (Cl, Br, I) are an important branch. The coordination chemistry of Cu(I) or Ag(I) halides (X = Cl/Br/I) featuring d^{10} shell has been of interest for large structural variation and rich electronic and optical properties [4, 5]. Although metal–metal interactions influence the properties of hybrids, such interactions are not the inevitable outcome. A dramatic structural change in volume, rigidity, charge, symmetry of the basic inorganic phases can be reached by introduction of new organic templates called structural directing agents [6–10]. To our knowledge, inorganic haloclusters in hybrids tend to form 1-D chains [11] through evaporation and concentration of solutions at room temperature (RT) which promise less halogen disorder. Among the reported hybrids with chain-like inorganic arrangement, linear cations usually array along the chains. It is promising to tune the mineral phase to display interesting properties triggered by the interactions with a linear guest template.

The linear template, 1,ω-bis(3,3′-methylimidazolium)alkyl dibromide, linked by saturated carbon chains with distinct length is flexible and can adopt energy allowed conformations, and the halometal cluster can be templated by such cations. The templates carrying two active carbene precursors may bring more inter- and intra-molecular interactions and more possibility for formation of stable and metastable supramolecules. *N*-heterocyclic carbenes (NHCs), unlike carbenes that are too reactive to be isolated, are electronically and sterically stabilized and play an important role in organometallic chemistry and catalytic science [12–16]. Deprotonating of NHC precursors is a common way to synthesize NHCs [17–23]. Thus, utilization of such N-substituted imidazolium salt as template affords opportunity to explore the role of the counter cations in assembly and arrangement of halometal polyanions.

As extension of our research [24, 25], six NHCs precursors (table 1) based on templated complexes were used to investigate effects of linear imidazolium-based template, 1,ω-bis(3,3′-methylimidazolium)alkyl dibromide, on pure inorganic halometal clusters and reported herein. These compounds were further characterized with IR spectra and thermal properties.

Table 1. The structures and names of diimidazolium *N*-heterocycles.

Names	Schemes
1,1′-methylenebis(3-methyl-1H-imidazol-3-ium); abbr: $[C_1(Mim)_2]^{2+}$	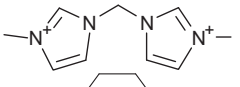
1,1′-(ethane-1,2-diyl)bis(3-methyl-1H-imidazol-3-ium); abbr: $[C_2(Mim)_2]^{2+}$	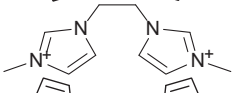
1,1′-(propane-1,3-diyl)bis(3-methyl-1H-imidazol-3-ium); abbr: $[C_3(Mim)_2]^{2+}$	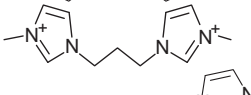
1,1′-(butane-1,4-diyl)bis(3-methyl-1H-imidazol-3-ium); abbr: $[C_4(Mim)_2]^{2+}$	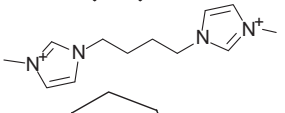
2,10-dimethyl-6,7-dihydro-5H-diimidazo [1,5-a:5′,1′-c][1,4]diazepine-2,10-diium; abbr: $[C_3'(Mim)_2]^{2+}$	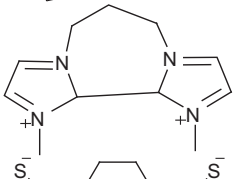
1,1′-(ethane-1,2-diyl)bis(3-methyl-1H-imidazol-3-ium-2-thiolate); abbr: $[C_2(Mim)_2S_2]$	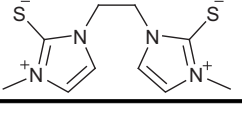

2. Experimental

2.1. *Materials and methods*

1,ω-bis(3,3′-methylimidazolium)alkyl dications ($\omega = 1$–4) were all prepared as bromide salt by direct alkylation of 1-methylimidazole with 1,ω-dibromoalkanes, while acetonitrile served as solvent [26]. Other chemicals and solvents were of analytical grade and obtained from commercial sources without purification. The IR spectrum was recorded on a Shimadzu IR435 spectrometer as KBr disk (4000–400 cm^{-1}). A model NETZSCHTG209 thermal analyzer was used to record simultaneous TG curves in flowing air at 30 mL/min at a heating rate of 5 °C/min to 800 °C using platinum crucibles.

2.2. *Synthesis*

2.2.1. Synthesis of 1. In a sealed tube to a solution of PbI_2 (0.1 mM) and KI (0.5 mM) in DMF a solution of KI (0.5 mM) in DMF/CH_3OH (1 : 1, v/v, 10 mL) was added dropwise and slowly to keep the interface clear. Then a solution of $C_4(Mim)_2{\cdot}2Br$ (0.1 mM, 38.0 mg) in CH_3OH (5 mL) was added carefully to the system. The reaction mixture was allowed to stand at RT for about a week in the dark. Yellow crystals suitable for X-ray single crystal diffraction analysis were collected in 75% yield. IR (KBr): 3447(s), 3086(w), 1629(w), 1588(m), 1559(m), 1450(w), 1423(m), 1161(s), 817(s), 732(s), 617(s), 614(s) cm^{-1}.

2.2.2. Synthesis of 2. The procedure was similar to the synthesis of **1** with the solution of $C_1(Mim)_2{\cdot}2Br$ (0.1 mM) in CH_3OH (5 mL) being added dropwise into solution of AgI (0.1 mM) and KI (0.5 mM) in DMF. Keeping at RT for about a week in the dark resulted in white crystals suitable for X-ray single crystal diffraction 60% yield. IR (KBr, cm^{-1}): 3131(m), 1654(m), 1611(s), 1581(m), 1547(s), 1442(s), 1427(s), 1385(s), 1164(s), 1085(s) cm^{-1}.

2.2.3. Synthesis of 3. The procedure was similar to the synthesis of **1** with solution of $C_3(Mim)_2{\cdot}2Br$ (1.0 mM) in CH_3OH (5 mL) being added dropwise into solution of AgI (0.1 mM) and KI (0.5 mM) in DMF. White crystals suitable for X-ray single crystal diffraction analysis were collected in 45% yield. IR (KBr): 3149(W), 3095(m), 2975(m), 2865(m), 1645(m), 1578(m), 1562(m), 1455(m), 1172(s), 622(s) cm^{-1}.

2.2.4. Synthesis of 4. The procedure was similar to the synthesis of **1** with solution of $C_4(Mim)_2{\cdot}2Br$ (1.0 mM) in CH_3OH (5 mL) being added dropwise into solution of AgI (0.1 mM) and KI (0.5 mM) in DMF. White crystals suitable for X-ray single crystal diffraction analysis were collected in 63% yield. IR (KBr): 3462(w), 3135(m), 3102(m), 3078(s), 2943(w), 1580(m), 1563(s), 1458(m), 1161(s), 827(s), 820(s), 816(m), 732(s), 615(s), 610(m) cm^{-1}.

2.2.5. Synthesis of 5. The procedure was similar to the synthesis of **1** with solution of $C_3(Mim)_2{\cdot}2Br$ (1.0 mM) in CH_3OH (5 mL) being added dropwise into solution of CuBr (0.1 mM) and KBr (0.5 mM) in DMF. Yellow crystals suitable for X-ray single crystal diffraction analysis were collected in 40% yield. IR (KBr): 3107(s), 3088(s), 2945(w),

1675(m), 1557(s), 1544(m), 1445(m), 1412(m), 1373(m), 1244(m), 1189(m), 1077(w), 1039(m), 796(s), 778(s), 719(s), 667(s), 517(m) cm^{-1}.

2.2.6. Synthesis of 6. $(NH_4)_2MoO_2S_2$ (0.3 mM), CuI (0.2 mM), and $C_2(Mim)_2{\cdot}2Br$ (0.4 mM) were ground in an agate mortar and dissolved in 30 mL of DMF; the solution was transferred to a flask and stirred for 10 h at 90 °C. The final solution was filtered and maintained in the dark. About three months later, deep-red crystals were obtained (yield 45%). IR (KBr): 3447(s), 3093(m), 1654(w), 1565(m), 1478(m), 1419(m), 1402(m), 1251(s), 1200(m), 1142(w), 1092(w), 731(s), 671(s), 611(w), 507(m) cm^{-1}.

2.3. *X-ray crystallography study*

Crystallographic data for **1–6** were collected at RT on a Bruker APEX-II area detector diffractometer equipped with graphite-monochromated Mo-Kα radiation ($\lambda = 0.71073$ Å). The structures were solved by direct methods and expanded using Fourier techniques. Non-hydrogen atoms were refined with anisotropic thermal parameters. The hydrogens were assigned with common isotropic displacement factors and included in the final refinement by using geometrical constraints. The structures were refined with full-matrix least-squares techniques on F^2 using SHELXTL-97 [27]. Crystallographic data and structural refinement details for **1–6** are summarized in table 2. Selected bond lengths and angles of **1–6** are summarized in table 3.

3. Results and discussions

3.1. *Synthesis*

Crystallization of many halometallates were attempted separately with **1**, ω-bis(3,3′-methylimidazolium)alkyl ($\omega = 1$–6) dibromide but only crystals of **1–6** were obtained. Remarkably, we found a seven-membered ring formed via formation of a C–C bond of the carbene precursor $[C_3(Mim)_2]^{2+}$ in the structure of **5**, and the cyclization product $[C_3'(Mim)_2]^{2+}$ of the NHC precursor was first reported in this paper [scheme 1(a)]. When we investigated the Mo(W)/Cu/S cluster-based hybrids [28(a)] assembled with the four title templates, structure **6** was realized, in which the carbene precursor $[C_2(Mim)_2]$ reacted with S from $(NH_4)_2MoO_2S_2$ (as a sulfur source) in the presence of CuI to form C–S bond *in situ*, resembling the reaction of carbenes with O and S atoms [28(b)] [scheme 1(b)]. Except for the template effect, $[C_2(Mim)_2S_2]$ in **6** also is a thiolate ligand to coordinate with Cu_2I_2 to generate the 2-D framework. There is no such interesting structure without NHCs reactions and so **6** could be regarded as the first polyrotaxane example featuring the biimidazolium thiolate cation ligand. New bonds (C–C or C–S) are formed via C–H activation. We assume that copper(I) acted as catalyst in air in formation of **5** and **6**, and the reported analogs [29] in which copper(I) has the same role agreed with our results.

3.2. *Crystal structures*

3.2.1. Crystal structure of $\{[C_4(Mim)_2](Pb_2I_6)\}_n$ (1). As shown in figure 1(a), **1** features chain-like $(Pb_2I_6)_n$ polyanions and organic dications. Each Pb is six-coordinate with six μ_2-I in octahedral geometry [2]. There are two crystallographically independent Pb^{2+} ions, and

Table 2. Crystallographic data and structural refinements details for **1–6**.

Compound	**1**	**2**	**3**	**4**	**5**	**6**
Formula	$C_{12}H_{20}I_6N_4Pb_2$	$C_9H_{14}Ag_2I_4N_4$	$C_{5.5}H_9AgI_2N_2$	$C_{12}H_{20}Ag_2I_4N_4$	$C_{11}H_{16}Br_3CuN_4$	$C_5H_7CuIN_2S$
Formula weight	1396.10	901.58	464.82	943.66	507.55	317.63
Temperature (K)	293(2)	293(2)	293(2)	293(2)	291.15	293(2)
Crystal system	Monoclinic	Orthorhombic	Monoclinic	Triclinic	Orthorhombic	Monoclinic
Space group	*P2(1)/n*	*P212121*	*P2/c*	*P-1*	$Pna2_1$	*P21/c*
a (Å)	8.0330(3)	9.8858(3)	9.4029(2)	9.2328(5)	15.5222(7)	9.8933(3)
b (Å)	15.3152(7)	13.8631(3)	7.4553(2)	11.1843(5)	10.4164(4)	10.5815(3)
c (Å)	11.5057(5)	14.4606(4)	15.0164(4)	12.3225(7)	9.8234(4)	7.8841(3)
α (°)	90.00	90.00	90.00	93.454(4)	90.00	90.00
β (°)	99.681(4)	90.00	92.101(2)	105.210(5)	90.00	104.979(4)
γ (°)	90.00	90.00	90.00	113.307(5)	90.00	90.00
V (Å^3)	1395.35(10)	1981.79(10)	1051.96(5)	1108.19(10)	1588.30(11)	797.31(5)
Z	2	4	4	2	4	4
ρ_{Calcd} (mg/mm^3)	3.323	3.022	2.935	2.828	2.123	2.646
F (0 0 0)	1204	1608	836	852	976	596
Crystal size (mm)	0.23 × 0.15 × 0.13	0.24 × 0.21 × 0.18	0.23 × 0.20 × 0.17	0.20 × 0.17 × 0.15	0.20 × 0.18 × 0.18	0.23 × 0.19 × 0.15
θ Range for data collection (°)	2.96–25.50	3.18–25.50	3.05–25.49	3.26–25.50	6.28–52.74	3.30–25.48
Reflections collected/unique	8727/2592	6942/3496	3689/1958	7629/4115	4179/2205	5218/1475
R(int)	0.0286	0.0359	0.0218	0.0275	0.0341	0.0308
Data/restraints/parameters	2592/0/113	3496/0/175	1958/0/99	4115/0/201	2205/1/175	1475/0/92
Goodness of fit on F^2	1.082	1.022	1.021	1.039	1.021	1.063
Final *R* indices [$I > 2\sigma(I)$]	$R1 = 0.0302$, $wR2 = 0.0728$	$R1 = 0.0343$, $wR2 = 0.0684$	$R1 = 0.0284$, $wR2 = 0.0598$	$R1 = 0.0380$, $wR2 = 0.0784$	$R1 = 0.0360$, $wR2 = 0.0639$	$R1 = 0.0476$, $wR2 = 0.1184$
R indices (all data)	$R1 = 0.0389$, $wR2 = 0.0765$	$R1 = 0.0423$, $wR2 = 0.0726$	$R1 = 0.0369$, $wR2 = 0.0645$	$R1 = 0.0504$, $wR2 = 0.0840$	$R1 = 0.0489$, $wR2 = 0.0680$	$R1 = 0.0540$, $wR2 = 0.1229$

Table 3. Selected bond distances (Å) and angles (°) for **1–6**.

Compound **1**					
Pb1–I2	3.1902(5)	Pb1–I1	3.2347(5)	Pb2–I1	3.2405(5)
Pb1–I3	3.2232(5)	Pb2–I3	3.2111(5)	Pb2–I2	3.2793(6)
I2–Pb1–I3	87.06(1)	I3–Pb1–I1^{i}	95.06(1)	I1^{ii}–Pb2–I2^{ii}	84.06(1)
I2–Pb1–I3^{i}	92.93(1)	I3–Pb1–I1	84.93(1)	I1–Pb2–I2^{ii}	95.93(1)
I2–Pb1–I1^{i}	94.39(1)	I3–Pb2–I1^{ii}	94.96(1)	I1^{ii}–Pb2–I2	95.93(1)
I2–Pb1–I1	85.60(1)	I3–Pb2–I1	85.03(1)	I1–Pb2–I2	84.06(1)
Compound **2**					
Ag1–I1	2.8319(9)	Ag2–I2	2.8147(9)	Ag2–I1	2.8910(9)
Ag1–I2	2.8428(9)	Ag2–I3	2.8467(9)	Ag1–Ag2	3.213(1)
Ag1–I4^{i}	2.8524(9)	Ag2–I4	2.8672(9)	Ag2–Ag1	3.718(1)
I1–Ag1–I2	111.53(3)	I3–Ag2–I4	99.03(3)	Ag1–I1–Ag2	68.31(2)
I4^{i}–Ag1–I3^{i}	98.61(3)	I2–Ag2–I1	110.61(3)	Ag2–I2–Ag1	69.22(2)
I1–Ag1–I4^{i}	112.08(3)	I2–Ag2–I4	110.60(3)	Ag2–I3–Ag1^{ii}	81.00(3)
I2–Ag1–I3^{i}	107.58(3)	I3–Ag2–I1	109.22(3)	Ag1^{ii}–I4–Ag2	81.10(3)
Compound **3**					
Ag1–I2	2.8538(5)	Ag2–I2^{i}	2.8626(5)	Ag2–I1^{ii}	2.8661(5)
Ag1–I1	2.8832(5)	Ag2–I2	2.8626(5)	Ag2–I1^{iii}	2.8661(5)
I2^{i}–Ag1–I2	103.16(2)	I1–Ag1–I1^{i}	94.36(2)	Ag2^{iv}–I1–Ag1	85.28(2)
I2^{i}–Ag2–I2	102.72(2)	I1^{ii}–Ag2–I1^{iii}	95.09(2)	Ag1–I2–Ag2	77.06(2)
Compound **4**					
Ag1–I1	2.8373(8)	Ag1–I1^{i}	2.8848(9)	Ag2–I4	2.8808(8)
Ag1–I2	2.8413(8)	Ag2–I2	2.8549(8)	Ag2–I3	2.8868(8)
Ag1–I3	2.8796(8)	Ag2–I4^{ii}	2.8752(8)	Ag1–Ag1^{i}	3.314(1)
I1–Ag1–I2	110.87(3)	I2–Ag2–I4^{ii}	127.58(3)	Ag1–I1–Ag1^{i}	70.80(3)
I1–Ag1–I3	115.82(3)	I2–Ag2–I4	104.33(2)	Ag1–I2–Ag2	77.07(2)
I2–Ag1–I3	103.74(3)	I4^{ii}–Ag2–I4	95.10(2)	Ag1–I3–Ag2	75.96(2)
I1–Ag1–I1^{i}	109.20(2)	I2–Ag2–I3	103.21(2)	Ag2^{ii}–I4–Ag2	84.90(2)
Compound **5**					
Br1–Cu1	2.370(1)	Br2–Cu1	2.3937(9)	Br3–Cu1	2.335(1)
C1–C2	1.34(1)	C3–C4	1.445(9)	C5–C6	1.35(1)
C1–N1	1.336(9)	C3–N1	1.328(7)	C4–N3	1.342(9)
C2–N2	1.358(9)	C3–N2	1.31(1)	C4–N4	1.336(8)
Br1–Cu1–Br2	114.24(4)	N2–C3–C4	121.3(6)	N4–C7–C8	114.5(6)
Br3–Cu1–Br1	125.50(4)	N4–C4–C3	122.7(7)	C7–C8–C9	116.0(7)
Br3–Cu1–Br2	120.18(4)	C5–C6–N4	107.5(7)	N2–C9–C8	113.2(7)
Compound **6**					
Cu1–S1^{i}	2.415(3)	Cu1–I1	2.650(2)	S1–C2	1.705(8)
Cu1–S1	2.434(3)	S1–Cu1^{iii}	2.415(2)		
S1^{i}–Cu1–S1	109.07(7)	Cu1–I1–Cu1^{ii}	71.77(5)	C2–S1–Cu1^{iii}	104.8(3)
S1–Cu1–I1	109.37(8)	Cu1^{iii}–S1–Cu1	148.7(1)	C2–S1–Cu1	97.0(3)

Symmetry codes for **1**: (i) $-x, -y+1, -z+1$ (ii) $-x+1, -y+1, -z+1$ (iii) $-x, -y+2, -z+1$; Symmetry codes for **2**: (i) $-x+1, y-1/2, -z+1/2$ (ii) $-x+1, y+1/2, -z+1/2$; Symmetry codes for **3**: (i) $-x+1, y, -z+1/2$ (ii) $x, y+1, z$ (iii) $-x+1, y+1, -z+1/2$ (iv) $x, y-1, z$; Symmetry codes for **4**: (i) $-x+1, -y+1, -z+1$ (ii) $-x, -y, -z$; Symmetry codes for **5**: (i) $-x, -y, z+1/2$ (ii) $-x+1/2, y+1/2, z+1/2$; Symmetry codes for **6**: (i) $x, -y+1/2, z+1/2$ (ii) $-x, -y, -z+2$ (iii) $x, -y+1/2, z-1/2$.

the alternative arrangement extends the ions into chains. The bond distances of Pb(1)···Pb (2) and Pb(1)···Pb(2)# are 4.016 or 4.017 Å, longer than the sum of the van der Waals radii of Pb^{2+} (3.62 Å), proving the absence of a Pb–Pb bond. The length of Pb–I ranges from 3.1902 to 3.2793 Å. The bond angles of Pb–I–Pb are 76.673°–77.253° and the bond angle of I–Pb–I are 84.068°–95.932°. It is in channels surrounded by regular dications where the polyanions are located, as shown in figure 1(b).

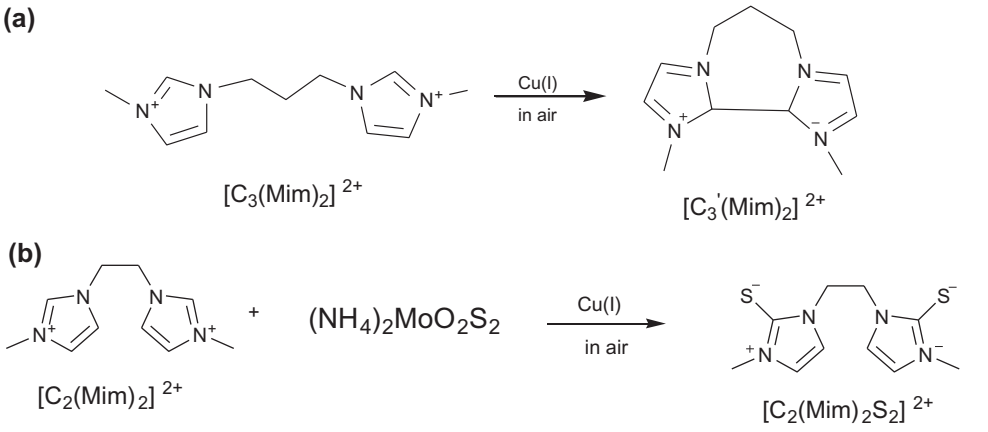

Scheme 1. (a) Schematic representation of the cyclization of imidazolium salt $[C_3(Mim)_2]^{2+}$ occurring during crystallization of **5**. (b) Schematic representation of the C–S bond formation in imidazolium salt $[C_2(Mim)_2]$ occurring during crystallization of **6**.

3.2.2. Crystal structure of $\{[C_1(Mim)_2]\ (Ag_2I_4)\}_n$ (2). As shown in figure 2(a), the μ_2-I connects two crystallographic independent silver ions and the alternative arrangement of Ag (1) and Ag(2) extend the ions into 1-D chains. The Ag–I distances are 2.8147–2.8911 Å. The Ag–I–Ag bond angles are 68.31(2)°–81.10(3)° and the I–Ag–I bond angles are 98.61 (3)°–116.32(3)°, indicating distorted tetrahedral geometry. The Ag(1)–Ag(2) bond length is 3.214 Å, which is shorter than the sum of the van der Waals radii of Ag (3.50 Å) and indicates the presence of Ag–Ag interaction; Ag(2)–Ag(1)# is 3.719 Å, which is longer than 3.50 Å and indicates the absence of Ag–Ag interaction. These Ag–Ag interactions occurred in the chain alternatively and emphasized the uniqueness of this compound compared with reported linear AgI chains with continuous Ag–Ag interactions [3(a)] or without Ag–Ag interactions [3(b) and (c)]. All the organic dications stand in regular packing mode along those chains to balance charge, as shown in figure 2(b).

3.2.3. Crystal structure of $\{[C_3(Mim)_2](Ag_2I_4)\}_n$ (3). The structure consists of organic dications and $(Ag_2I_4)_n$ polyanions trapped in the channels formed by the dications [figure 3(a)]. Through Ag coordination with four μ_2-I in tetrahedral geometry, polyanions are extended into 1-D chains similar with that in **2** except Ag–Ag interaction. Ag(1) and Ag(2) extend alternatively along the inorganic chains. The Ag···Ag distance is 3.561 or 3.894 Å, both of which are longer than the sum of the van der Waals radii of Ag^+ [3(b) and (c)]. The Ag–I–Ag bond angles are 85.275° and 77.061° and the I–Ag–I bond angles are 94.36°–118.37°. The channels surrounded by dications accommodate the inorganic chains [figure 3(b)].

3.2.4. Crystal structure of $\{[C_4(Mim)_2](Ag_2I_4)\}_n$ (4). Similar with **3**, **4** features chain-like polyanions and flexible dications surround them as shown in figure 4(a). Each Ag is four-coordinate with μ_2-I forming a tetrahedron and iodide bridging to combine Ag ions forming an infinite chain. Two crystallographic independent silver ions stack in Ag(1)–Ag(1)–Ag (2)–Ag(2)–Ag(1)–Ag(1) mode along the inorganic chains. The Ag–Ag distances in Ag(1)–Ag(1)#, Ag(1)–Ag(2), and Ag(2)–Ag(2)# are 3.315, 3.549, and 3.885 Å, respectively, and

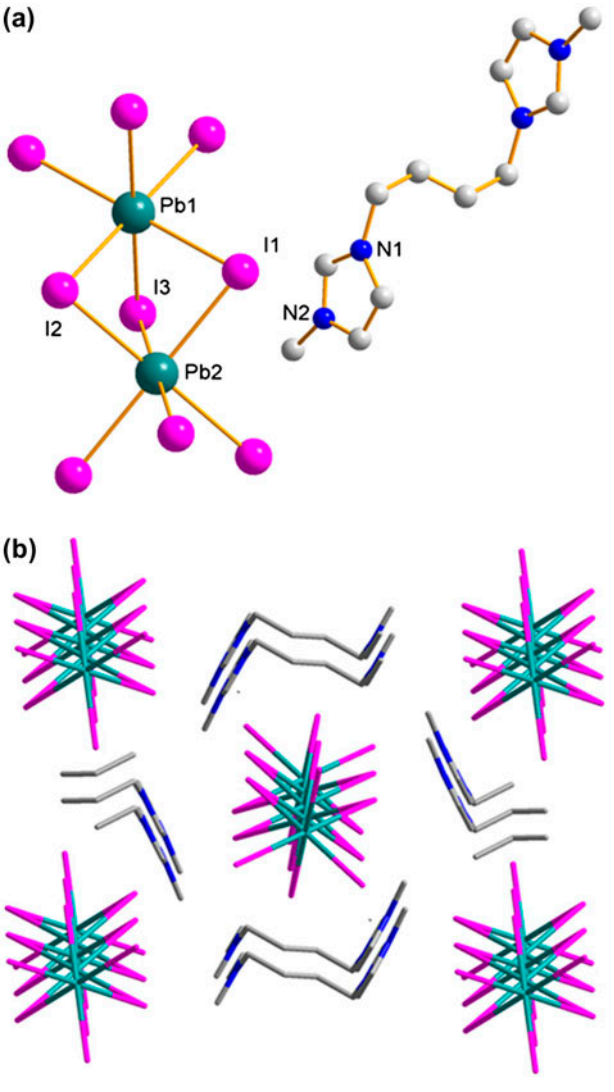

Figure 1. (a) The unit structure of **1** (symmetry codes: #1 $-x$, $-y+1$, $-z+1$; #2 $-x+1$, $-y+1$, $-z+1$; #3 $-x$, $-y+2$, $-z+1$). (b) The 3-D packing architecture of **1**.

show no evident Ag–Ag interactions. The Ag–I bond lengths are 2.837–2.887 Å and the I–Ag–I bond angles are 103.74°–115.82°, which show us the distorted tetrahedron due to the effect of the organic dications via weak interactions. The Ag–I–Ag bond angles are 70.80°–84.90°. The polyanions are embraced by the *trans* dications, as shown in figure 4(b).

3.2.5. Crystal structure of {[C_3′(Mim)$_2$] ($CuBr_3$)} (5). The unit structure of **5** consists of one Cu coordinated with three μ-Br [8] and one dication [figure 5(a)]. The C–H···Br short contacts hold the components together. In comparison with **3**, the original dication converted into a seven-membered-ring product via C–C coupling in the presence of CuBr

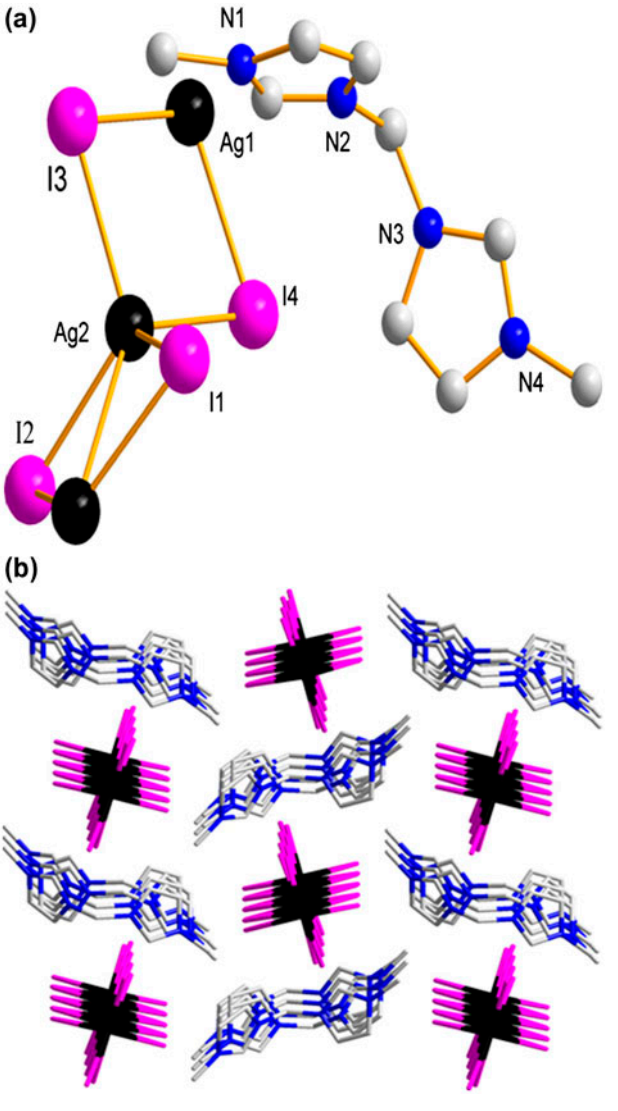

Figure 2. (a) The unit structure of **2** (symmetry codes: #1 $-x+1$, $y-1/2$, $-z+1/2$; #2 $-x+1$, $y+1/2$, $-z+1/2$). (b) The 3-D packing architecture of **2**.

instead of AgI. According to the literature [29, 30–32(a)], $[C_3(Mim)_2]$ was oxidized by oxygen in air catalyzed by Cu(I), proving the high activity of NHCs precursors. The Cu–Br bond lengths are 2.336–2.394 Å and the Br–Cu–Br bond angles 114.24°–125.50°, which both indicate the template effect of organic cation on the triangle geometry of the metal by Cu–Br···H bonds and electrostatic interactions [figure 5(b)].

3.2.6. Crystal structure of $\{[C_2(Mim)_2S_2]_2(Cu_2I_2)\}_n$ (6). The X-ray single-crystal structure shows that **6** crystallizes in the monoclinic system with the space group *P21/c*. The unit structure of **6** is shown in figure 6(a). In this structure there exists a 12-member ring

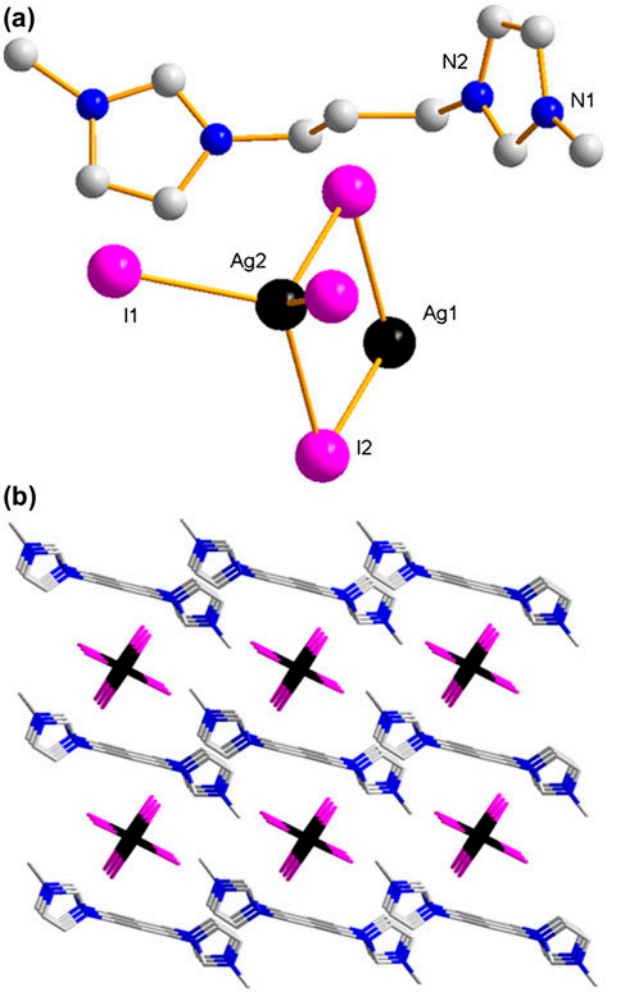

Figure 3. (a) The unit structure of **3** (symmetry codes: #1 $-x+1$, y, $-z+1/2$; #2 x, $y+1$, z; #3 $-x+1$, $y+1$, $-z+1/2$; #4 x, $y-1$, z; #5 $-x$, y, $-z+1/2$). (b) The 3-D packing architecture of **3**.

molecular box and related rotaxane structure [figure 6(b)]. Two Cu ions coordinating with two μ_2-I [Cu–I, 2.650(1) Å] form a four-member ring. It is μ_2-S coordinating to copper [Cu–S, 2.415(3) or 2.434(3) Å] that bridge to connect above building blocks into the 12-member ring $(–Cu–I–Cu–S–Cu–S–)_2$, and extend into a 2-D network. In each molecular ring, anti-configurational $[C_2(Mim)_2S_2]$ formed via the C–H bond activation of the NHC precursor and the formation of S1–C2 bonds and then all the cations were connected with inorganic anions. In other words, each molecular ring was penetrated by the $[C_2(Mim)_2S_2]$ ligand at the loosest point, thus a 2-D coordination polymer framework based on the formation of a pseudorotaxane by threading of the 12-member molecular wheel with $[C_2(Mim)_2S_2]$ string axle formed. Topologically, the network can be identified as a 2-D (6, 3) net, shown in figure 6(c).

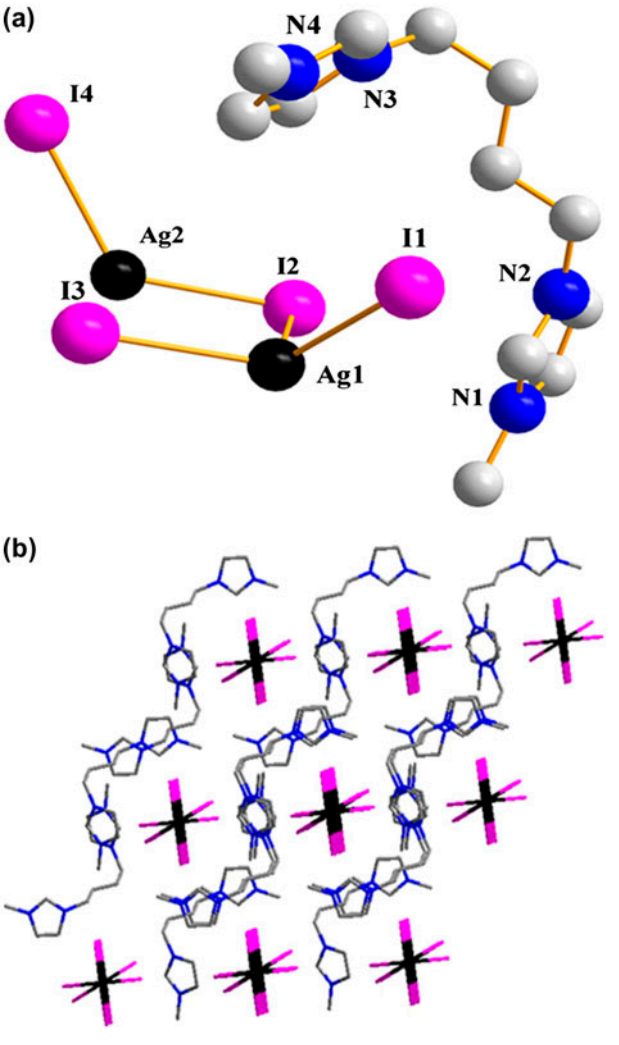

Figure 4. (a) The unit structure of **4** (symmetry codes: #1 $-x+1$, $-y+1$, $-z+1$; #2 $-x$, $-y$, $-z$). (b) The 3-D packing architecture of **4**.

3.3. *TGA*

In order to investigate the relation between weak interactions/metal–metal interactions and the thermostability of lead/cuprous/silver halides, the TGA experiments of **1–6** were carried out up to 900 °C in flowing air. The TG curves of **1–6** are shown in figure S1(a–f), see online supplemental material at http://dx.doi.org/10.1080/00958972.2014.908288. The decomposition of **1** mainly proceeded in two stages. The first stage took place from 300 to 425 °C and probably corresponds to elimination of dications $[C_4(Mim)_2]$; the second stage from 495 to 860 °C mainly involved burning of the inorganic framework. The TG data showed that the decomposition of **2** took place from 265 to 440 °C (related to the elimination of organic cations $[C_1(Mim)_2]$). The mass decreased sharply after 675 °C to the end.

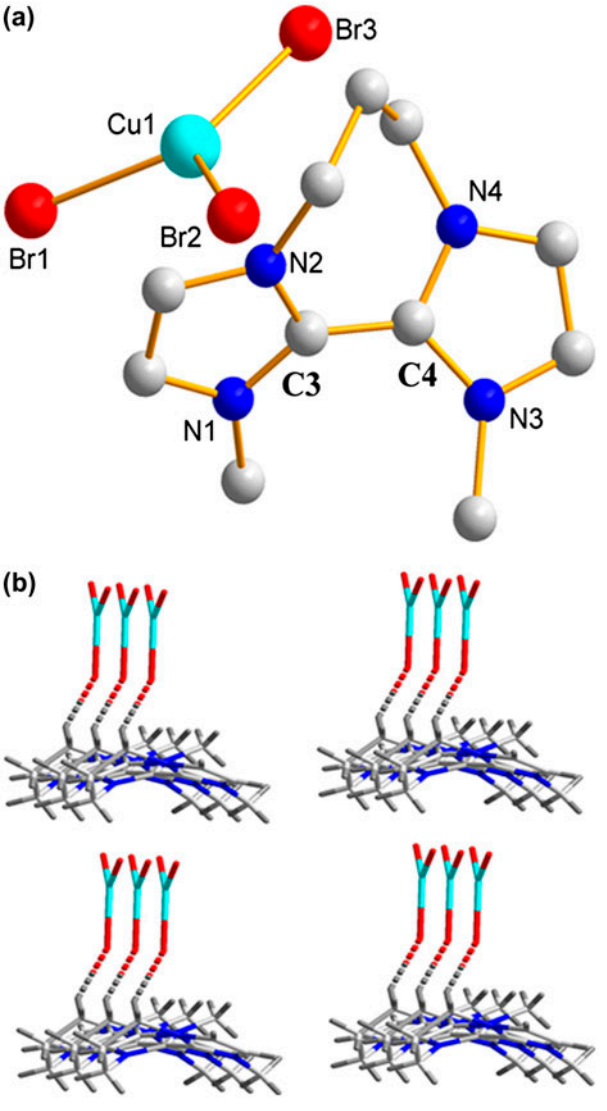

Figure 5. (a) The unit structure of **5**. (b) The 3-D packing architecture of **5**.

As the TG curve shows, decomposition of **3** took place at 300–440 °C and 440–635 °C, which correspondingly related to elimination of organic cations $[C_3(Mim)_2]$ and the extreme burning of the inorganic component. Similarly, decomposition of **4** took place from 296 to 425 °C because of the loss of organic cation $[C_4(Mim)_2]$. The mass decreased from 680 °C to the end, due to burning of the inorganic materials. The TG curve of **5** showed that the decomposition took place at 220–420 °C corresponding to decomposition of organic cations. From 655 °C to the end the mass decreased because of the inorganic burning. The TG curve of **6** showed that the organic cations decomposed at 280–385 °C, and the inorganic frameworks were burned from 495 °C to the end with the mass decreasing continually.

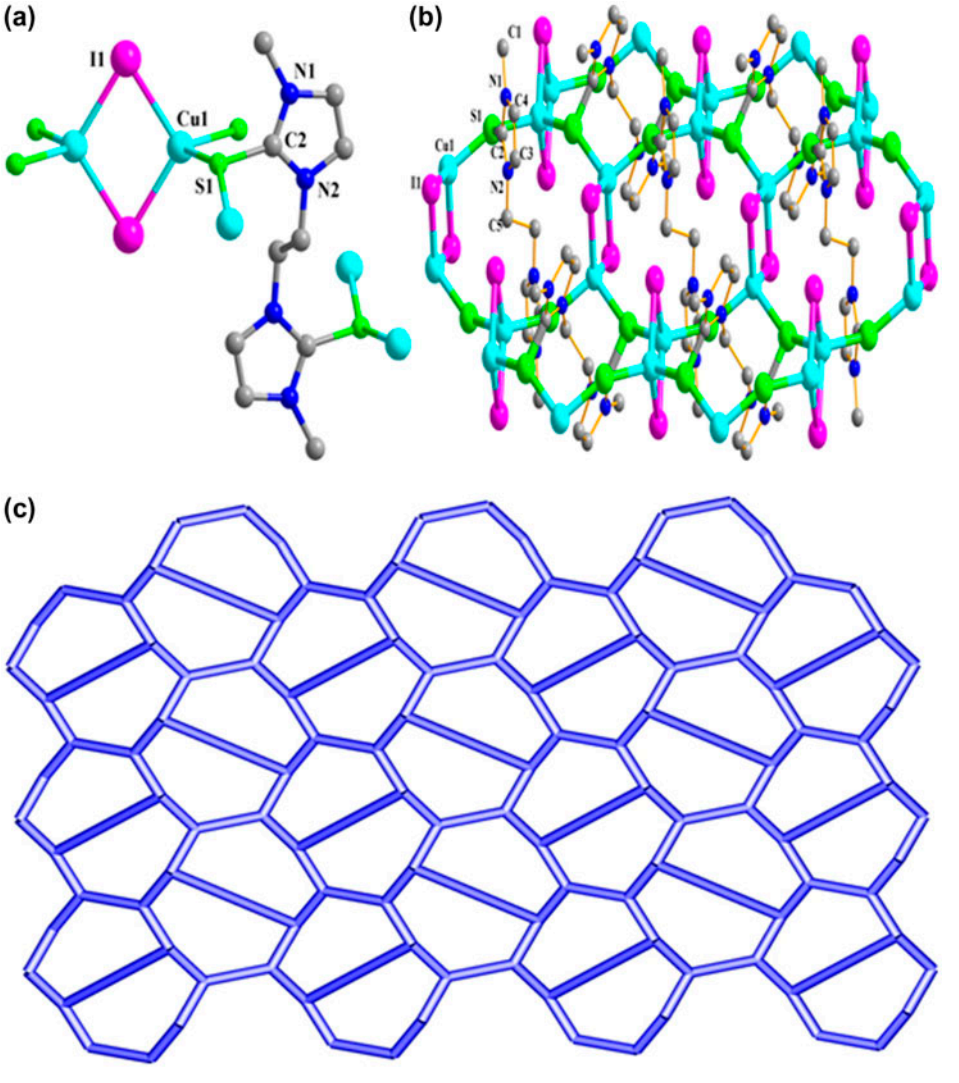

Figure 6. (a) The unit structure of **6** (symmetry codes: #1 x, $-y+1/2$, $z+1/2$; #2 $-x$, $-y$, $-z+2$; #3 x, $-y+1/2$, $z-1/2$; #4 $-x$, $-y+1$, $-z+2$). (b) The two-layer packing architecture of **6**. (c) View of the coordination environment of Cu in **6** along the *a*-direction, showing the (6,3) topology.

Thermal behavior of **1–4** and **6** are similar and the loss of organic dications mainly occurred near 300 °C, which means weak interactions such as C–H···I/Br have limited influence on thermostabilities. In contrast, the initial decomposition temperature of **5** decreased (far below 300 °C), indicating a lower thermal stability of the NHC cyclization product $[C_3'(Mim)_2]^{2+}$. There are residues of **2**, **4**, and **6** at 900 °C compared with **1**, **3**, and **5** which are consistent with the existence of metal–metal interactions or coordination bonds in the former.

4. Conclusion

We prepared six halometal complexes templated by linear imidazolium-based organic cations 1,ω-bis(3,3′-methylimidazolium)alkyl dibromide. Similar carbene precursor and metal–NHC complexes were reported by Özdemir *et al.* [32(b) and (c)] and our work showed that the metal halides (PbI_2, AgI, CuBr, and CuI) were not ideal metal bases for formation of NHC complexes. From the six crystal structures of **1–6**, different templates make differences to the coordination environment of the transition metal ions. Compounds **2**, **3**, and **4** possess similar 1-D chain structures with different organic cations trapped. We found that Ag1–Ag2 bonds exist only in **2**; **3** or **4**, induced by the smaller NHC precursor [$C_1(Mim)_2$], and show different cations have special effects on polyanions, and smaller organic cations may facilitate formation of the Ag···Ag interactions via hydrogen bonds and electrostatic interactions. Unexpectedly, oxidative coupling reactions occur to both NHCs precursors among **5** and **6** with copper(I). $[C_3(Mim)_2]^{2+}$ in **5** has been changed to a seven-membered ring via double C–H activation in the presence of Cu(I) and air; the seven-membered ring is stabilized by conjugation. $[C_2(Mim)_2S_2]$ in **6** forms C–S bonds *in situ* via C–H activation catalyzed by Cu(I) under air, and the thiolate is a bridge to coordinate with Cu_2I_2 generating a 2-D organic framework. Although a series of bication-templated inorganic polymeric nets have been described [33–36], **5** has a different and more interesting structure than those. Compound **6** may be regarded as the first polyrotaxane example featuring the biimidazolium thiolate cation ligand. Further research about the mechanism and reactions of NHCs precursors' is currently underway.

Supplementary material

CCDC reference numbers 871217–871222 contain the supplementary crystallographic data for **1–6**. These data can be obtained free of charge via http://www.ccdc.cam.ac.uk/conts/retrieving.html, or from the Cambridge Crystallographic Data Center, 12 Union Road, Cambridge CB21EZ, UK; Fax: +44 1223 336 033 or E-mail: deposit@ccdc.cam.ac.uk.

Funding

We greatly acknowledge the financial support by NSFC [grant number 21171148], [grant number J1103309].

References

[1] O.M. Yaghi, H. Li, C. Davis, D. Richardson, T.L. Groy. *Acc. Chem. Res.*, **31**, 474 (1998).
[2] (a) H.B. Duan, H.R. Zhao, X.M. Ren, H. Zhou, Z.F. Tian, W.Q. Jin. *Discuss. Faraday Soc.*, **40**, 1672 (2011); (b) S. Mishra, E. Jeanneau, S. Daniele, G. Ledoux, P.N. Swamy. *Inorg. Chem.*, **47**, 9333 (2008); (c) Y. Chen, Z. Yang, C.X. Guo, C.Y. Ni, H.X. Li, Z.G. Ren, J.P. Lang. *CrystEngComm.*, **13**, 243 (2011); (d) S. Mishra, E. Jeanneau, O. Iasco, G. Ledoux, D. Luneau, S. Daniele. *Eur. J. Inorg. Chem.*, **2012**, 2749 (2012); (e) H. Krautscheid, C. Lode, F. Vielsack, H. Vollmer. *J. Chem. Soc., Dalton Trans.*, 1099 (2001); (f) Z.J. Tang, A.M. Guloy. *J. Am. Chem. Soc.*, **121**, 452 (1999).
[3] (a) C. Chen, H.Y. Qiu, W.Z. Chen, D.Q. Wang. *J. Organomet. Chem.*, **693**, 3273 (2008); (b) J.M. Yue, W.J. Wang, W.Z. Fu, X.N. Han, Z.H. Zhang, L.F. Wang, Y.Y. Niu. *Synth. React. Inorg. Met.-Org. Nano-Met. Chem.*, **41**, 100 (2011); (c) J.Z. Huo, Z.X. Zhao, M.C. Shi, H.L. Li, Q.X. Liu. *Acta Cryst.*, **E68**, m787 (2012).
[4] D.B. Mitzi. *Prog. Inorg. Chem.*, **48**, 1 (1999).

[5] Y.Y. Niu, H.G. Zheng, H.W. Hou, X.Q. Xin. *Coord. Chem. Rev.*, **248**, 169 (2004).
[6] Y.Y. Niu, B.L. Wu, X.L. Guo, Y.L. Song, X.C. Liu, H.Y. Zhang, H.W. Hou, C.Y. Niu, S.W. Ng. *Cryst. Growth Des.*, **8**, 2393 (2008).
[7] H.H. Li, Z.R. Chen, J.Q. Li, C.C. Huang, Y.F. Zhang, G.X. Jia. *Cryst. Growth Des.*, **6**, 1813 (2006).
[8] (a) C. Zimmermann, F.W. Heinemann, A. Grohmann. *Eur. J. Inorg. Chem.*, **8**, 547 (2001); (b) G.A. Bowmaker, A. Camus, B.W. Skelton, A.H. White. *J. Chem. Soc., Dalton Trans.*, 727 (1990); (c) E. Deiters, V. Bulach, M.W. Hosseini. *New J. Chem.*, **32**, 99 (2008); (d) C. Hasselgren, S. Jagner, I. Dance. *Chem. Eur. J.*, **8**, 1269 (2002).
[9] X.M. Jiang, M.J. Zhang, H.Y. Zeng, G.C. Guo, J.S. Huang. *J. Am. Chem. Soc.*, **133**, 3410 (2011).
[10] Y. Chen, Z.O. Wang, Z. Yang, Z.G. Ren, H.X. Li, J.P. Lang. *Dalton Trans.*, 9476 (2010).
[11] J.W. Cheng, S.T. Zheng, G.Y. Yang. *Inorg. Chem.*, **46**, 10261 (2007).
[12] F. Glorius, S. Bellemin-Laponnaz. *Top. Organomet. Chem.*, **21**, 5 (2007).
[13] G. Bertrand. *Carbene Chemistry*, Marcel Dekker Inc., New York, NY (2002).
[14] M. Melaimi, M. Soleilhavoup, G. Bertrand. *Angew. Chem. Int. Ed.*, **49**, 8810 (2010).
[15] O. Schuster, L. Yang, H.G. Raubenheimer, M. Albrecht. *Chem. Rev.*, **109**, 3445 (2009).
[16] K. Öfele, E. Tosh, C. Taubmann, W.A. Herrmann. *Chem. Rev.*, **109**, 3408 (2009).
[17] H.W. Wanzlick. *Angew. Chem. Int. Ed. Engl.*, **1**, 75 (1962).
[18] H.W. Wanzlick, H.J. Schönherr. *Angew. Chem. Int. Ed. Engl.*, **7**, 141 (1968).
[19] K. Öfele. *J. Organomet. Chem.*, **12**, P42 (1968).
[20] A.J. Arduengo, R.L. Harlow, M. Kline. *J. Am. Chem. Soc.*, **113**, 361 (1991).
[21] T. Dröge, F. Glorius. *Angew. Chem. Int. Ed.*, **49**, 6940 (2010).
[22] W.A. Herrmann, M. Elison, J. Fischer, C. Köcher, G.R.J. Artus. *Angew. Chem. Int. Ed. Engl.*, **34**, 2371 (1995).
[23] L. Benhamou, E. Chardon, G. Lavigne, S.P. Bellemin-Laponnaz, V. César. *Chem. Rev.*, **111**, 2705 (2011).
[24] M.R. Grimmett. *Imidazole and Benzimidazole Synthesis*, Academic Press, San Diego, CA (1997).
[25] H.J. Du, Z.Z. Shu, Y.Y. Niu, L.S. Song, Y. Zhu. *J. Solid State Chem.*, **190**, 296 (2012).
[26] (a) S. Ahrens, T. Strassner. *Inorg. Chim. Acta*, **359**, 4789 (2006); (b) J. Vitz, D.H. Mac, S. Legoupy. *Green Chem.*, **9**, 431 (2007).
[27] G.M. Sheldrick. *SHELXTL-97, Program for Crystal Structure Refinement*, University of Gottingen, Germany (1997).
[28] (a) Y.Y. Niu, Y.L. Song, H.G. Zheng, D.L. Long, H.K. Fun, X.Q. Xin. *New J. Chem.*, **25**, 945 (2001); (b) M. Arbelot, A. Allouche, K.F. Purcell, M. Chanon. *J. Org. Chem.*, **60**, 2330 (1995).
[29] E. Boess, C. Schmitz, M. Klussmann. *J. Am. Chem. Soc.*, **134**, 5317 (2012).
[30] H.Q. Do, O. Daugulis. *J. Am. Chem. Soc.*, **129**, 12404 (2007).
[31] D. Zhao, W. Wang, F. Yang, J. Lan, L. Yang, G. Gao, J. You. *Angew. Chem. Int. Ed.*, **48**, 3296 (2009).
[32] (a) Y. Li, J. Jin, W.X. Qian, W.L. Bao. *Org. Biomol. Chem.*, **8**, 326 (2010); (b) B. Yigit, Y. Gök, İ. Özdemir, S. Günal. *J. Coord. Chem.*, **65**, 371 (2012); (c) S. Demir, İ. Özdemir, B. Çetinkaya, E. Şahin, C. Arici. *J. Coord. Chem.*, **64**, 2565 (2011).
[33] Y.Y. Niu, B.L. Wu, X.L. Guo, Y.L. Song, X.C. Liu, H.Y. Zhang, H.W. Hou, C.Y. Niu, S.W. Ng. *Cryst. Growth Des.*, **8**, 2393 (2008).
[34] J.M. Yue, Y.Y. Niu, B. Zhang, S.W. Ng, H.W. Hou. *CrystEngComm.*, **13**, 2571 (2011).
[35] Y.Z. Qiao, J.M. Yue, X.C. Liu, Y.Y. Niu. *CrystEngComm.*, **13**, 6885 (2011).
[36] Y.Z. Qiao, W.Z. Fu, J.M. Yue, X.C. Liu, Y.Y. Niu, H.W. Hou. *CrystEngComm.*, **14**, 3241 (2012).